Test of An UCAV Air Inlet Duct (Eikon) at Static Conditions in FOI Suckdown Facility

Ingemar Samuelsson

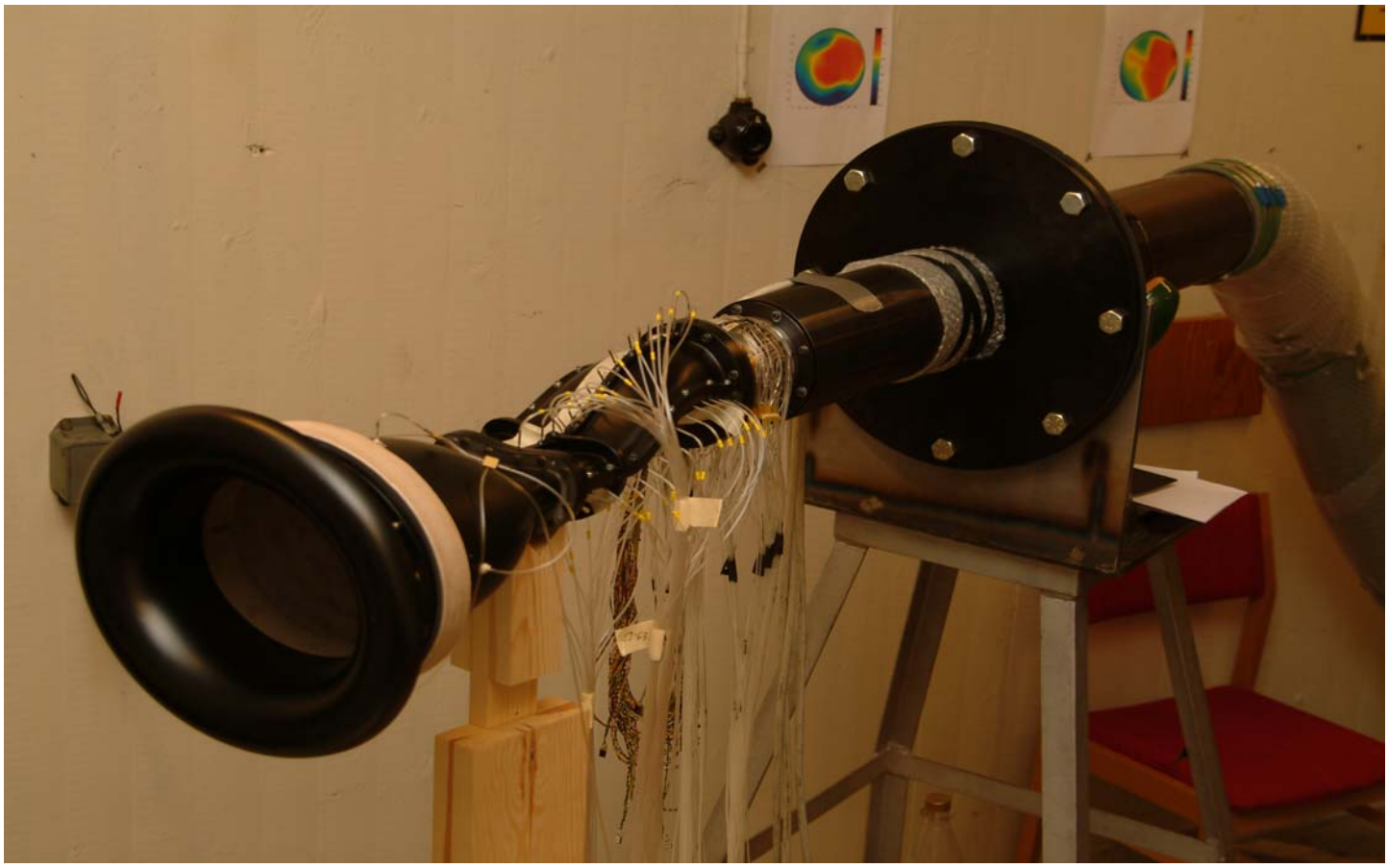

FOI-R-- 1572 --SE
ISSN 1650-1942

Systems Technology
Technical report

November 2005

FOI is an assignment-based authority under the Ministry of Defence. The core activities are research, method and technology development, as well as studies for the use of defence and security. The organization employs around 1350 people of whom around 950 are researchers. This makes FOI the largest research institute in Sweden. FOI provides its customers with leading expertise in a large number of fields such as security-policy studies and analyses in defence and security, assessment of different types of threats, systems for control and management of crises, protection against and management of hazardous substances, IT-security and the potential of new sensors.

FOI
Defence Research Agency
Systems Technology
SE-164 90 Stockholm

Phone: +46 8 555 030 00
Fax: +46 8 555 031 00

www.foi.se

Test of An UCAV Air Inlet Duct (Eikon) at Static Conditions in FOI Suckdown Facility

Contents

Nomenclature

A	area	[m^2]
A_{throat}	area of the inlet throat ($A_{throat} = 3.4878 \cdot 10^{-3}$ m^2)	[m^2]
c	speed of sound ($c = \sqrt{\gamma RT}$)	[m/s]
D_{AIP}	diameter of the AIP ($D_{AIP} = 0.07083$ m)	[m]
DC_{60}	dimensionless total pressure distortion index (based on the AIP worst 60° degree sector, for definition see Ref. [2]	[-]
L_{throat}	Reynolds number reference length ($L_{throat} = \sqrt{\frac{4 \cdot A_{throat}}{\pi}} \approx 0.0666$ m)	[m]
$\dot{m}$	duct mass flow rate	[kg/s]
M	Mach number ($M = \frac{U}{c}$)	[-]
M_{AIP}	Mach number at the AIP (based on duct mass flow rate by means of the equation: $\dot{m} = \frac{\sqrt{\gamma} M_{AIP}}{\left(1 + \frac{\gamma - 1}{2} M_{AIP}^2\right)^{\frac{\gamma+1}{2(\gamma-1)}}} \cdot \frac{p_{0AIP} A_{Aip}}{\sqrt{RT_0}}$)	[-]
M_{throat}	Mach number at the inlet throat (based on duct mass flow rate by means of the equation: $\dot{m} = \frac{\sqrt{\gamma} M_{throat}}{\left(1 + \frac{\gamma - 1}{2} M_{throat}^2\right)^{\frac{\gamma+1}{2(\gamma-1)}}} \cdot \frac{p_{0ref} A_{throat}}{\sqrt{RT_0}}$)	[-]
p	static pressure	[Pa]
p_0	total pressure	[Pa]
$p_0^{'}$	fluctuating part of the total pressure (with zero mean value)	[Pa]
p_{0AIP}	AIP total pressure mean ($p_{0AIP} = \frac{1}{40} \sum_{i=1}^{40} p_0(i)$, where $p_0(i)$ $(i = 1, 40)$ are the total pressures measured by the measuring cell)	[Pa]
p_{0ref}	reference total pressure in the onset flow, $p_{0ref} = p_{atm} - \Delta p$	[Pa]
p_{atm}	ambient (atmospheric) pressure	[Pa]
p_{avg}	average AIP wall static pressure (= mean of four measured static pressures)	[Pa]
$P_{recovery}, P_R$	(total) pressure recovery ($P_{recovery} = \frac{p_{0AIP}}{p_{0ref}}$)	[-]
R	gas constant ($R \approx 287$ J/(kgK) for air)	[J/kg/K]
Re_{throat}	throat Reynolds number ($Re_{throat} = \frac{\rho_{throat} U_{throat} L_{throat}}{\mu_{throat}}$)	[-]
T	static temperature	[K]
T_0	total temperature	[K]
U_{throat}	axial velocity in the throat	[m/s]
(x, y, z)	Cartesian coordinates (x : axial, y : transverse: z : vertical)	[m,m,m]
Δp	pressure difference over the screens in the settling chamber	[Pa]
φ_0	angle of rotation of the measuring cell	[°]

γ	specific heat ratio ($\gamma = 1.4$ for air)	[-]
μ	dynamic viscosity (μ_{throat} : the dynamic viscosity in the throat flow)	[kg/m/s]
ρ	density (ρ_{throat} : the density in the throat flow)	[kg/m^3]

Abbreviations

AIP	Aerodynamic Interface Plane
ESP	Electronically Scanned Pressure
PSD	Power Spectral Density
PSI	Pressure System Inc.
RMS	Root Mean Square
RPM	Rapid Prototype Manufacturing
UCAV	Unmanned (Uninhabited) Combat Aerial Vehicle

1. Introduction, background

The present report shows some results from a rig test of an UCAV air inlet duct model. The test is a subproject to the FoT25 project entitled 'Propulsion Integration (Framdrivningsintegration)', where one of the objectives is to build up an aerodynamic design/analysis capability of 'stealthy' air inlets. The means chosen to this aim are mainly CFD simulations and experimental tests. The experiments comprise tests at static conditions (that is, without free stream)(present report) as well as forthcoming wind tunnel tests with a fore-body model. The present test served the principal purpose of being a 'pretest' in order to get acquainted with the prevalent duct aerodynamics and to sort out any measurement problems. It also served the purpose as a first check of the CFD design and analysis of the aerodynamics of the tested duct geometry. However, the present report is concerned with the experimental results only.

2. Model

The basic diffuser duct geometry is shown in Figure 1 (full scale dimensions (in meter)).
As can be seen in Figure 1, the inlet to the diffuser is kidney shaped. The diffuser is rather short (diffuser length / D_{AIP} = 2.5) with S-bends both at the upper and the lower walls.

The model scale was determined by the size of the available measuring cell. This cell has an inlet diameter of 0.073 m (the AIP diameter of the cell is 0.07083 m) and since the full scale design diameter at the AIP is about 0.660 m, the model scale is 1:9.05.

Since the test was to be carried out at static conditions, that is, without free stream, it was necessary to provide a bellmouth to the inlet for a smooth inflow. At the upstream end a flare was attached, followed by a gauze frame (with metal gauzes at both ends). The gauze frame was attached to a settling chamber that smoothly contracts into the throat of the inlet. The purpose of the screens was to smooth out any non-uniform distribution of total pressure in the inlet flow.
The throat has a constant cross sectional area over a length equal to $\sqrt{4 \cdot A_{throat} / \pi}$ and it has the same cross sectional shape as the diffuser inlet.

Downstream of the diffuser, where the cross section is circular, the model is attached to the measuring cell.

The model arrangement is schematically depicted in Figure 2. (Please note that in Figures 1 and 2 the inlet geometry and model inlet arrangement are shown in the 'normal' (non-inverted) position, and not in the tested inverted position (with a roll of 180º)).

The model inlet was fabricated by means of RPM (Rapid Prototype Manufacturing) in plastic (separate parts: Flare, settling chamber, throat/diffuser duct). The flare and the settling chamber were manufactured in whole pieces while the throat/diffuser duct was manufactured into two parts for two reasons: Firstly, to facilitate photographing flow patterns in oil flow visualisation tests; secondly, for drilling and visual inspection of the pressure taps. After receiving the model parts and drilling of the pressure holes, the inlet was painted black (mainly as a protection from moisture, since the plastic is hygroscopic, but also for giving a good photographical contrast). The frame for the two screens (mesh width 0.56 mm and wire diameter 0.16 mm) was made of wood and the screens were glued onto the upstream and downstream ends of the frame.
The various parts of the inlet were bolted together and O-rings were used for sealing. Downstream of the most downstream screen four pitot tubes pointing upstream (not shown) were installed in the settling chamber. These tubes were interconnected and the resulting pressure was measured relative the ambient laboratory atmospheric pressure. This 'pneumatically averaged' total pressure served as a reference total pressure, p_{0ref}, for the inlet flow.

3. Model mounting, suction facility

For practical reasons the inlet was mounted 'upside down', as indicated in Figure 3. The measuring cell was installed at one end of a steel tube that was attached to a mounting steel flange (see Figure 4). The inlet was also supported by a wooden frame (visible in Figure 4) in order to lessen the attachment moment on the measuring cell due to the dead weight of the inlet. Downstream of the mounting flange a reinforced plastic hose (internal diameter 152 mm) was connected to an aluminium tube (internal diameter 140 mm). Five meters into this straight tube a mass flow meter was installed. This mass flow meter was an orifice plate with hole diameter of 100 mm. Downstream of the mass flow meter an additional aluminium tube (length = 2 m) was mounted and to this tube a plastic hose (length ≈ 10 meters) was connected. The plastic hose was then connected, via a control valve and a shut-off valve, to an evacuated rock chamber. Due to the downstream low pressure of about 20 kPa it was possible to choke the inlet flow.

4. Instrumentation and data acquisition

4.1 Measuring cell

The main instrumentation for this test consists of a so called measuring cell that measures total pressures (both steady-state and time-variant quantities) at the AIP (Aerodynamic Interface Plane), as well as wall static pressures. The steady-state pressures were measured by means of ESP modules. Figure 5a shows a photograph of the measuring cell.

The centres of the total pressure tubes are located at area weighted radii in five rings and at eight azimuthal positions (that is, with a pitch of 45º); hence, in all forty total pressures are measured at the chosen AIP position. The numbering and orientation of the pressure probes are indicated in Figure 5b. At each azimuthal position (that is, at each rake arm) also the flow swirl could be measured at middle and outermost radial positions by means of combined total pressure and flow direction probes. At these positions two obliquely cut (45º) pressure tubes were attached to the total pressure tube. The flow direction probes (and the total pressure tubes) were calibrated, for flow angle and Mach number dependence, prior to the test. Also, wall static pressures were measured at the same axial position as the total pressure at four azimuthal positions. There were also four wall boundary layer pressure probes, but these are not shown in Figure 5b.

In addition to the above-mentioned instrumentation for steady-state pressures, the measuring cell was also equipped with 24 Kulite transducers for the measurement of time-variant total pressures. The Kulites were arranged in eight three-probes arms, and were placed between the steady-state arms, see Figure 5b.

4.2 Duct wall static pressures

The static pressures on the inlet duct wall were measured along four lines (top, bottom and the two sides, see Figures 7 and 8). The pressures were measured by means of ESP modules (PSI) as absolute pressures. These modules were calibrated prior to each run.

4.3 Duct mass flow rate

The duct mass flow rate was measured by means of an orifice plate (upstream diameter = 0.140 m, orifice plate hole diameter = 0.100 m); the procedure followed was according to the one described in Ref. [1]. Here two pressure transducers were used to measure the upstream and downstream pressures, respectively. These transducers were calibrated prior to the test. The inlet flow temperature was measured by means of a thermistor placed in the laboratory hall about two metres upstream of the inlet bellmouth. The flow was assumed to be adiabatic.

4.4 Time-variant total pressures

The time-variant total pressures at the AIP were measured at 24 locations by means of Kulite probes (see Figure 5). The probes were provided with protection caps at the tips (protection from any particle impact on the sensors).

The Kulite probes were statically calibrated from about 50 kPa to about atmospheric pressure.

4.5 Atmosperic pressure and pressure difference over the screens

The ambient atmospheric pressure (p_{atm}) in the laboratory hall was measured by means of an electronic barometer. The pressure difference (Δp) over the screens in the settling chamber was measured by means of a separate differential pressure transducer. The reference total pressure for flow was calculated as the difference between these two measured pressures: $p_{0ref} = p_{atm} - \Delta p$.

4 6 Data acquisition

The data acquisition was carried out by means of the programming language LabView and acquisition cards (from National Instruments). At each selected duct mass flow rate the steady-state signals were multiplexed, amplified, filtered (low pass filters with cutoff frequency 10 Hz), averaged and stored.An in-house developed system was used for the ESP module calibration, data acquisition, averaging and storing

The time-variant total pressure signals were sampled, after amplification, at 20 kHz simultaneously with sample-and-hold circuits for slightly more than 2 seconds. This means that over one million of time-variant data points were acquired at each run. In addition the total pressure signals were also filtered with 4-pole Butterworth filters (-24 db/octave) with a cutoff frequency of 10 kHz. These filters are integral to the amplifiers.

5. Experimental procedure

It was noted that for the present kind of test, with a fixed geometry and with atmospheric conditions, the only parameter that can be varied is the duct mass flow rate. It was therefore decided to vary the mass flow rate from rather low values up to where the duct flow was choked. In order to express the degree of mass flow through the duct with a dimensionless quantity, a mass flow rate averaged throat Mach number M_{throat} was determined by using the expression for the mass flow rate in a one-dimensional duct:

$$\dot{m} = \frac{\sqrt{\gamma} M_{throat}}{\left[1 + \frac{\gamma - 1}{2} M_{throat}^2\right]^{\frac{\gamma+1}{2(\gamma-1)}}} \cdot \frac{p_{0ref} A_{throat}}{\sqrt{RT_0}}$$

From this equation one can calculate M_{throat} from the measured and known values of the mass flow rate $\dot{m}$, p_{0ref}, γ, R, T_0 and A_{throat}. This was carried out in real time during the runs and presented on a monitor.

It was decided to perform the test from M_{throat} = 0.20 in steps of 0.05 up to choking. Note that choking in this case is determined in an operational way by noting that the mass flow rate did not increase beyond a certain amount of opening of the control valve.

The experimental procedure was as follows:

- Evacuating the rock camber (minimum pressure: about 20 kPa)
- Calibrating the ESP modules
- Opening the inlet door to the air drying beds
- Opening the shut-off valve (letting the low-pressure in the rock chamber up to downstream end of the control valve)
- Manual opening and adjustment of the control valve to desired throat Mach number (read from monitor)
- Waiting a few seconds (for stabilization)
- Data acquisition (during about 10 seconds, for time-variant signal during about 2 seconds), averaging and storing
- Closing the shut-off valve
-

This procedure was carried out for each selected mass flow rate and for the three different orientations of the measuring cell (φ_0 = 0º, 11.25º and 22.5º).

6. Estimation of uncertainties

No extensive uncertainty analysis has been carried out for the obtained test results. However, a limited investigation of the uncertainty of the mass flow rate has been performed. In [Ref. 1] expressions are given for determination of the mass flow rate uncertainties; the calculations are based both on bias of the underlying calibration of the mass flow meter (that is, uncertainty in the discharge coefficient) and the precision of the used sensors. One can notice the bias due to the discharge coefficient of the present mass flow meter (the orifice plate) is about 0.7 % (given in Ref. [1]). This value representing the minimum achievable uncertainty value, is probably a conservative estimate in Ref. [1]. If lower uncertainties are desired, one is forced to perform a separate calibration of the mass flow meter intended for use.

To obtain the total mass flow rate uncertainty, one must also add the transducer precision to the above given value of the calibration bias. For the cases investigated here, the total relative uncertainty in

mass flow rate amounts to about 1.6 % at M_{throat} = 0.20 to about 0.8 % at the highest throat Mach numbers.

7. Results and discussion

7.1 Scope of test

The extent of the test is summarized in Table 1. This table gives the main characteristics of each run, such as mass flow rate, reference total pressure, pressure recovery and distortion index. As can be seen from the table there are three main groups (with 9 runs each), where the throat Mach number has been varied (from 0.20 to 0.55); the difference between the groups is the value of the parameter φ_0 (0º, 22.5º and 11.25º, respectively (in that order)). This parameter φ_0 is the angular rotation of the measuring cell relative the diffuser duct, that is, how the arms of the cell are oriented relative the flow. As can be seen from the tabulated values this has a certain influence on for instance the calculated pressure recovery. The reason for this is probably an insufficient spatial sampling of the flow total pressure distribution by the tubes in the measuring cell. In this report, however, only results with φ_0 = 11.25º are presented.

Finally there are also some repeat runs.

7.2 Total pressure distributions at AIP (Figure 6)

Figure 6 shows the total pressure distributions (normalized with the reference total pressure) over the AIP for nine different mass flow rates. The data are for φ_0=11.25º where the rakes of the measuring cell are symmetrically located over the AIP. The positions of the individual pressures are marked with crosses (×). The data are shown as colour plots as well as with contour lines (plotted by means of MATLAB). As can be seen the overall total pressure losses increase with mass flow rate (or equivalently, with throat Mach number). There are some distinct features visible in the plots:

- At the top there is a region where the total pressure decreases quite substantially with mass flow rate (of the order of 20% to 30% of the reference pressure). This is interpreted as an effect of separated flow in the upper S-bend of the duct, probably due to boundary layer separation caused by the rather steep adverse pressure gradient on the upper duct wall (see Figure 7).
- At the bottom area of the duct there seems to exist two depressions in the total pressure distribution on both sides of the duct vertical symmetry plane. This is thought to be due to the existence of two vortices emanating from separated flow in the lower S-bend at the beginning of the diffuser. The total pressure defect in these vortices is not as high as the corresponding defect found at the upper side of the diffuser. From this one can suggest that in order to lessen the pressure losses by means of some flow control (e.g. vortex generators) it might be more efficient to do so on the upper diffuser wall, since the possible gains can be higher.

In connection with these results it was observed that at the highest mass flow rate the flow seemed to be choked, since it was not possible to obtain any higher mass flow rate by further opening of the control valve. The question now is, where in the duct does the choking occur? From Table 1, one can note, for Run no. 8012 (with throat Mach number = 0.5494) and where choking is thought to exist, that the calculated Mach number at the AIP is about 0.506 (based on measured mass flow rate, average AIP total pressure and area). This could indicate that the choking occurs somewhere in the duct between the throat and the AIP or, perhaps more likely, that the choking occurs near the probe support arms just downstream of the AIP. At the locations of these the arms the duct is abrubtly enlarged; the idea behind this was to try to compensate for the blockage of the arms. However, since the flow very likely separates from the edge where the duct area increases, the area compensation idea

does not work. No further investigation of this was however pursued during the test. Perhaps a detailed analysis by means of numerical calculations could shed some light on this.

7.3 Duct wall static pressure distributions (Figures 7 and 8)

Figure 7 shows the duct wall static pressure distributions along duct top and bottom lines at varying mass flow rates. As can be seen there are two regions which exhibit rather large pressure gradients, in the vicinity of the upper and lower S-bends. For both these regions there are adverse pressure gradients in the downstream direction. This confirms, at least to some degree, the observations made from the AIP total pressure distributions.

Figure 8 shows the corresponding static pressure distributions along the duct wall sides. One notes that the port and starboard distributions are similar (which they should be, due to the symmetrical geometry, indicating that the onset flow likewise is symmetrical). For the side line pressures the pressure gradients are smaller than along the top and bottom lines, which seems intuitively correct since the geometry is much more slowly varying in the streamwise direction.

7.4 Pressure recovery (Figure 9)

Figure 9 shows the pressure recovery versus throat Mach number for $\varphi_0 = 11.25^\circ$. There is gradual decrease in pressure recovery with increasing Mach number, which again confirms the observation made from the total pressure distributions. Over the tested range of mass flow rate, the pressure recovery varies from 99.1 % down to 93.6 %.

7.5 Distortion index DC_{60} (Figure 10)

Figure 10 shows the distortion index DC_{60} versus throat Mach number. With increasing mass flow rate the distortion seems to increase, which also is consistent with the appearances of the total pressure distribution. As the mass flow rate goes up also the total losses increase, thereby increasing the spatial non-uniformities of the total pressure distribution, giving a higher distortion.

7.6 Time-variant total pressure (Figure 11)

No detailed analysis of the acquired unsteady total pressure data has been carried out. Only a few selected results are presented here.

Figures 11(a, b and c) show the times series of the unsteady total pressure, histogram and the power spectral density, respectively, for Kulite No.14 at throat Mach number 0.4. For the time series, where data are sampled with 20 kHz, the fluctuating part is shown normalized with the average total pressure. One can notice that the amplitude varies from –15 % to about +12 % (approximately). This means that sometimes the absolute values of the unsteady total pressure is higher than the reference total pressure in the onset flow (about 4 % of the samples are above the reference pressure). In Figure 11a) also the standard deviation of the fluctuations are plotted (± 4.9 %, about).

In Figure 11b the corresponding histogram of the signal is shown. Here one notices two distinct peaks separated about two standard deviations in amplitude. This can perhaps indicate that the signal contains a strong sinusoidal component superimposed on a more or less random signal. In Figure 11c, depicting the PSD of the signal, it is evident that there is a rather sharp peak at about 469 Hz, verifying the above conjecture. Here one can only guess about the reason for this behaviour of the signal. Perhaps the separated flow exhibits a very strong periodical pattern, for instance swinging from side to side (across the main flow direction) or there can be a pulsation in the axial direction or a combination of both. However, in order to gain a better insight into this flow behaviour, a more

detailed analysis is required of acquired data, probably also further experimental investigations are needed.

7.6.1 Power spectral densities (Figure 12)

Figure 12 shows the PSD of all the 24 unsteady total pressure signal for Run No. 8008 (throat Mach number = 0.4). Here the previously shown PSD for Kulite No. 14 (Figure 11c) is shown once more. Please note that there are two different vertical scales in the plots: For the Kulite signals Nos. 11, 12, 14 and 15 the vertical scale is ten times higher than for the other twenty signals. This is due to the fact that the signal contents in Nos. 11, 12, 14 and 15 are so much higher than for the rest of the signals. One can observe that the PSD:s for these four signals are very similar, both in shape and level, exhibiting a sharp peak at about 470 Hz. The other signals seem to be more or less flat without any marked peaks and with rather low spectral amplitudes. For Kulite Nos. 10 and 13 the levels are increased below 2 kHz, but the maximum levels for these signals are less than 10 % of the peak values for Kulites 11, 12, 14 and 15.

7.6.2 Root-mean-square distributions (Figure 13)

Figure 13 shows a compilation of colour coded distributions of RMS values for nine different throat Mach numbers. As can be seen there is a region at the top of the AIP where the RMS values of the total pressure variations increase in magnitude with increasing throat Mach number. At the bottom part there is also an increase in RMS magnitude with increase in throat Mach number, but not as marked as for the upper region. There seems to be a certain similarity with corresponding steady total pressure loss distributions shown in Figure 6, in that the largest total pressure losses occur in about same locations as the largest RMS values.
This behaviour is probably due to the fact that the underlying physics (e.g. flow separation) comprises unsteadiness as well as losses.

8. Conclusions

In this report a static (that is, at static conditions without free stream) test of an isolated air inlet is described and some of the obtained test results are presented and discussed. The inlet shape is thought to be typical for current UCAV configurations with a rather short S-shaped diffuser duct. In order to increase the line-of-sight blockage there are two S-bends (one on the upper part of the duct and one on the lower part).

The purpose of the presented test was principally to act as a ’pretest’ in order to get acquainted with the prevalent duct aerodynamics and to sort out any measurement problems. It also served the purpose as a first check of the CFD design and analysis of the aerodynamics of the tested duct geometry. However, the present report is concerned with the experimental results only.

The test comprised measurements of total pressure distributions at the AIP (as well as AIP wall static pressures) and inlet duct wall static pressures at different duct mass flow rates.

It was found that there is a gradual decrease of pressure recovery with increasing mass flow rate, from about 0.991 at throat Mach number ≈ 0.2 to 0.936 at throat Mach number ≈ 0.55. The total pressure distortion index DC_{60} increases with increasing throat Mach number.

At the highest mass flow rate the inlet flow seemed to be choked since it was not possible obtain a higher mass flow by further opening of the downstream control valve. No investigation, however, was pursued in order to find out where in duct this choking did occur. From the AIP total pressure distributions it was noted that the largest total pressure losses seemed to originate from the S-bend on the upper part of the duct. This could suggest that for enhancing the performance of the inlet one

could either redesign the diffuser upper geometry or apply some flow control (e.g. vortex generators) in this region or perhaps a combination of these proposed measures.

The time-invariant total pressure distributions exhibited increased amplitudes with increasing mass flow rates and the largest RMS values at the AIP occured at about where the losses in steady total pressure were largest. This is in some way consistent with the general experience that flow separation phenomena often are both unsteady and associated with losses. It was also found that the spectral content of the total pressure fluctuations was dominated by very sharp peaks at a particular frequency, perhaps indicating a periodical flow separation phenomenon.

References

[1] International Standard ISO 5167-1: "Measurement of fluid flow by means of pressure differential devices –
Part 1: Orifice plates, nozzles and Venturi tubes inserted in circular cross-section conduits running full"
First Edition 1991-12-15.

[2] Seddon, J and Goldsmith, E.L. "Intake Aerodynamics"
AIAA EDUCATION SERIES
ISBN 0-930403-03-7.

Run No.	φ_0 [°]	M_{throat}	M_{AIP}	p_{0ref} [Pa]	p_{avg} [Pa]	Re_{throat} $\times 10^{-6}$	duct mass flow rate [kg/s]	T_0 [K]	$P_{recovery}$	DC_{60}	p_{atm} [Pa]	Remarks
7972	0.00	0.2009	0.1784	100229	95039	0.287	0.2761	300.53	0.9914	0.1708	100465	
7973	0.00	0.2500	0.2227	100126	92182	0.354	0.3390	300.48	0.9865	0.1900	100465	
7974	0.00	0.3020	0.2698	100004	88332	0.421	0.4021	300.44	0.9804	0.1913	100465	
7975	0.00	0.3512	0.3147	99880	84153	0.482	0.4581	300.56	0.9737	0.2122	100461	
7976	0.00	0.4001	0.3607	99757	79263	0.541	0.5103	300.48	0.9648	0.2236	100460	
7977	0.00	0.4507	0.4092	99635	73269	0.597	0.5599	300.58	0.9550	0.2401	100461	
7978	0.00	0.4995	0.4577	99533	66657	0.647	0.6035	300.73	0.9441	0.2715	100466	
7979	0.00	0.5250	0.4833	99482	63572	0.674	0.6250	300.35	0.9388	0.2665	100458	
7980	0.00	0.5499	0.5070	99453	62096	0.698	0.6447	300.23	0.9357	0.2669	100447	
7993	22.50	0.2004	0.1779	98939	93846	0.283	0.2722	300.15	0.9922	0.1654	99174	
7994	22.50	0.2506	0.2229	98836	90924	0.350	0.3355	300.15	0.9874	0.1897	99175	
7995	22.50	0.3013	0.2686	98713	87253	0.416	0.3963	300.00	0.9820	0.2024	99169	
7996	22.50	0.3516	0.3145	98580	83025	0.478	0.4531	299.97	0.9755	0.2189	99161	
7997	22.50	0.4003	0.3597	98457	78208	0.534	0.5041	300.17	0.9674	0.2299	99159	
7998	22.50	0.4511	0.4079	98334	72209	0.591	0.5535	299.96	0.9581	0.2532	99160	
7999	22.50	0.5009	0.4570	98224	65563	0.641	0.5972	300.29	0.9472	0.2665	99157	
8000	22.50	0.5250	0.4796	98179	62689	0.665	0.6169	300.22	0.9440	0.2711	99150	
8001	22.50	0.5500	0.5026	98161	61286	0.689	0.6365	300.13	0.9416	0.2700	99147	
8003	11.25	0.2007	0.1783	98718	93613	0.283	0.2719	300.19	0.9914	0.1651	98954	
8005	11.25	0.2504	0.2230	98613	90743	0.348	0.3342	300.76	0.9864	0.1762	98953	
8006	11.25	0.3028	0.2705	98490	86941	0.416	0.3968	300.69	0.9804	0.2042	98951	
8007	11.25	0.3528	0.3165	98367	82687	0.477	0.4528	300.72	0.9727	0.2062	98951	
8008	11.25	0.4006	0.3613	98248	78023	0.534	0.5036	299.90	0.9646	0.2346	98951	
8009	11.25	0.4510	0.4095	98117	72110	0.588	0.5516	300.63	0.9550	0.2408	98944	
8010	11.25	0.5007	0.4588	98006	65511	0.639	0.5952	300.73	0.9440	0.2685	98940	
8011	11.25	0.5255	0.4835	97965	62520	0.663	0.6154	300.73	0.9390	0.2737	98938	
8012	11.25	0.5494	0.5061	97937	61180	0.685	0.6339	300.77	0.9362	0.2708	98926	
8017	0.00	0.4000	0.3598	98172	78051	0.531	0.5018	300.81	0.9667	0.2255	98882	Repeat of 7976
7967	11.25	0.4026	0.3629	99852	79073	0.546	0.5141	299.60	0.9647	0.2272	100560	" 8008
7963	22.50	0.4006	0.3600	100951	80152	0.546	0.5164	301.11	0.9674	0.2267	101660	" 7997
8015	0.00	0.2998	0.2675	98428	87115	0.412	0.3930	300.71	0.9815	0.1933	98884	" 7972
7966	11.25	0.3024	0.2699	100107	88399	0.424	0.4034	299.67	0.9808	0.1976	100568	" 8006
7962	22.50	0.3008	0.2682	101198	89518	0.424	0.4050	301.06	0.9819	0.1910	101656	" 7995

Table 1. List and summary of test runs

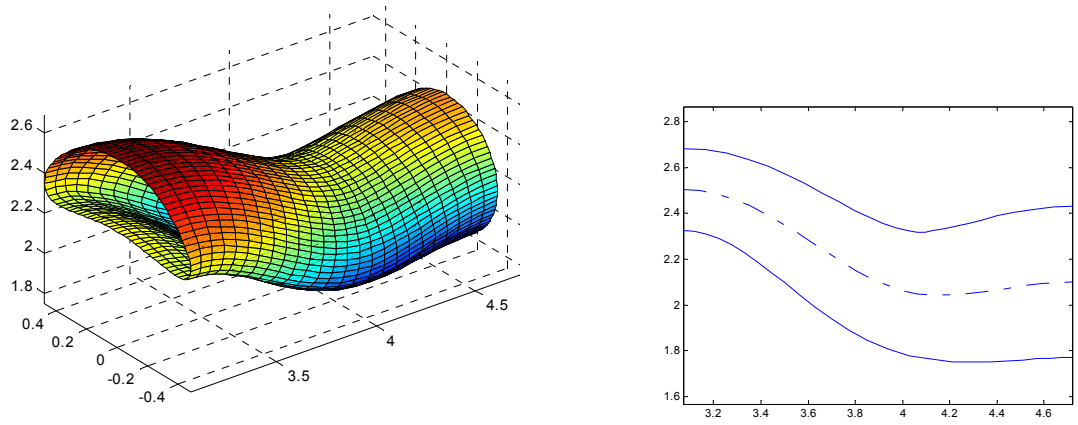

Figure 1. Basic diffuser duct geometry

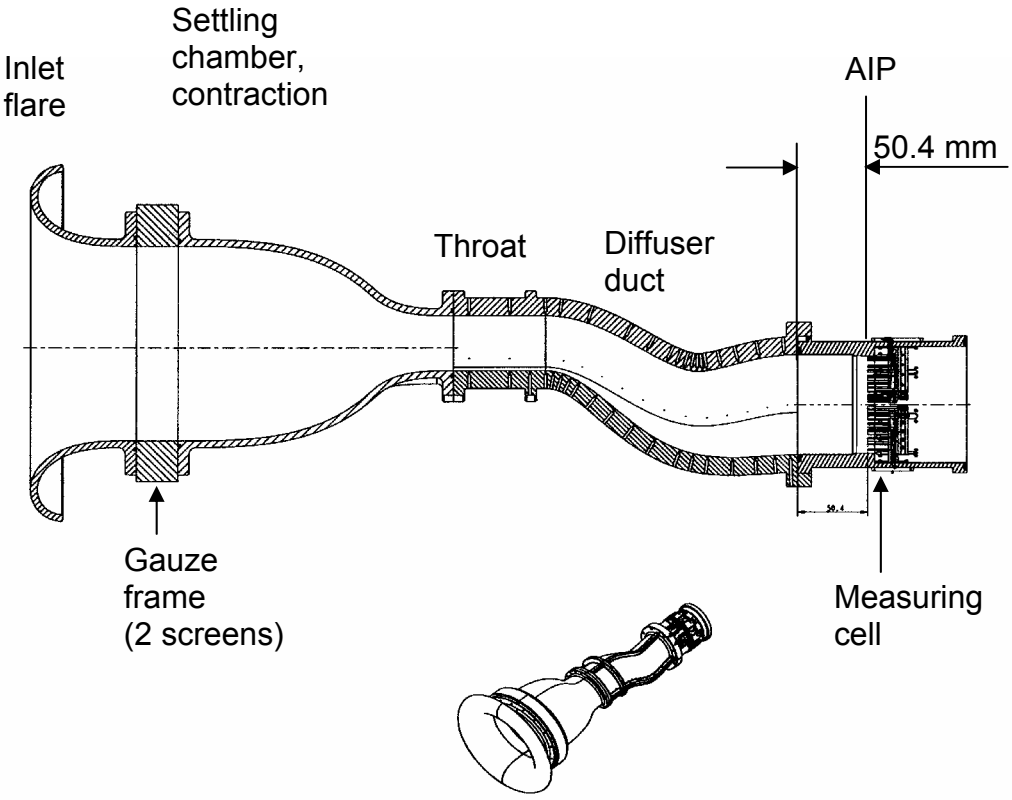

Figure 2. Model inlet arrangement

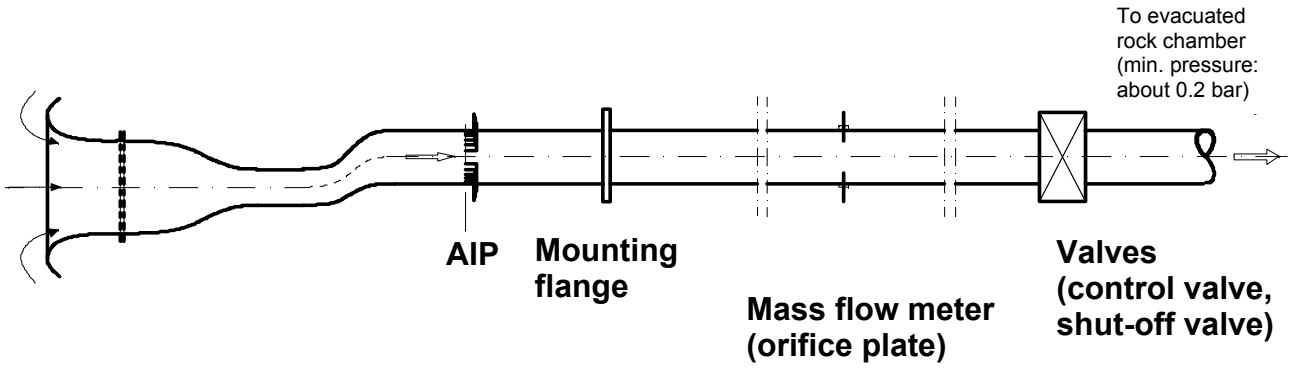

Figure 3. Schematic test setup

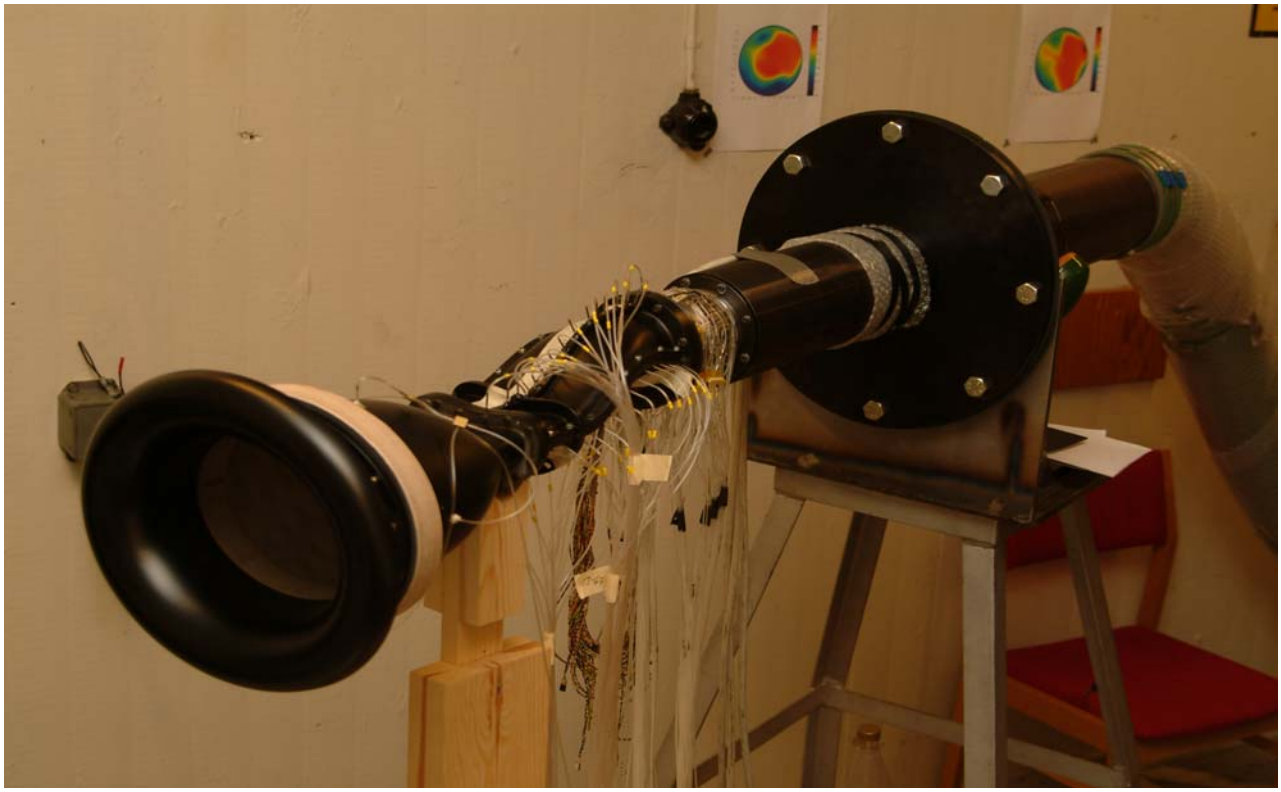

Figure 4. Photograph of model test set-up

a)

b)

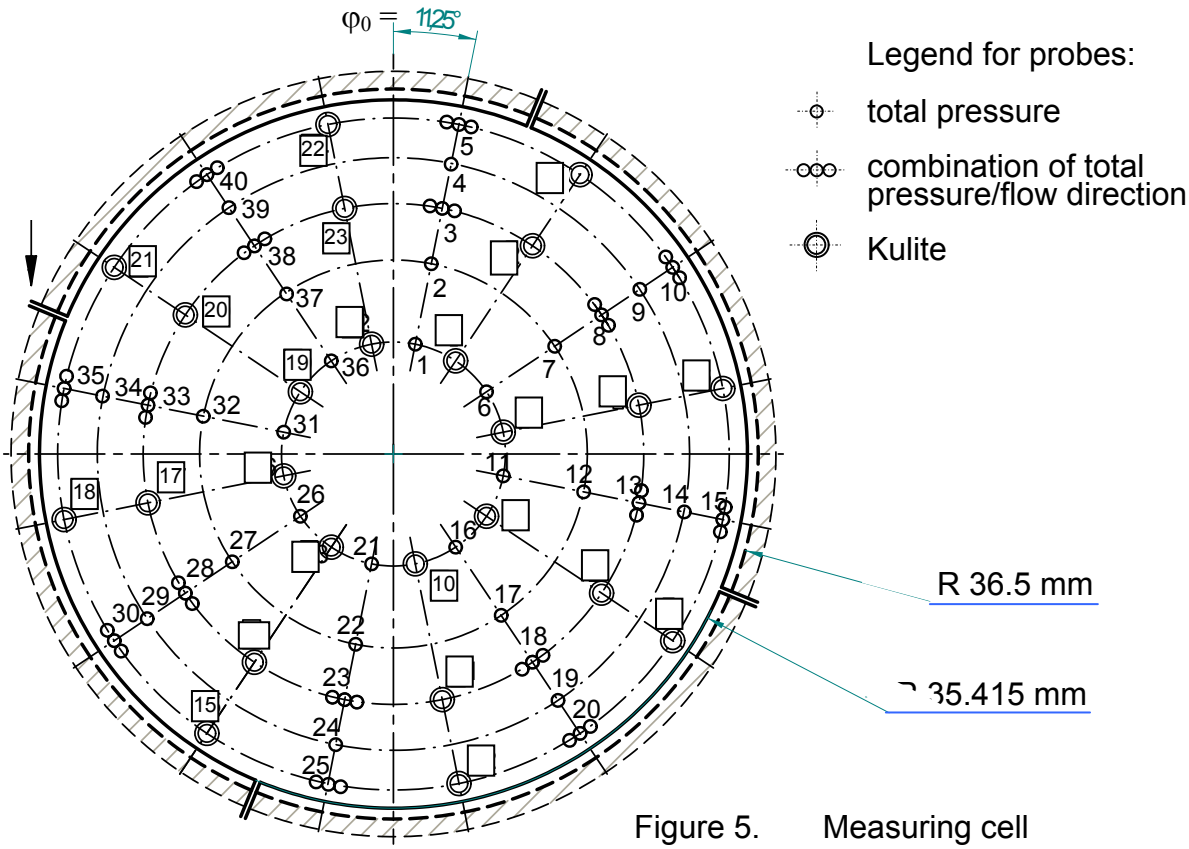

Figure 5. Measuring cell
a) Photograph
b) Distribution of probes

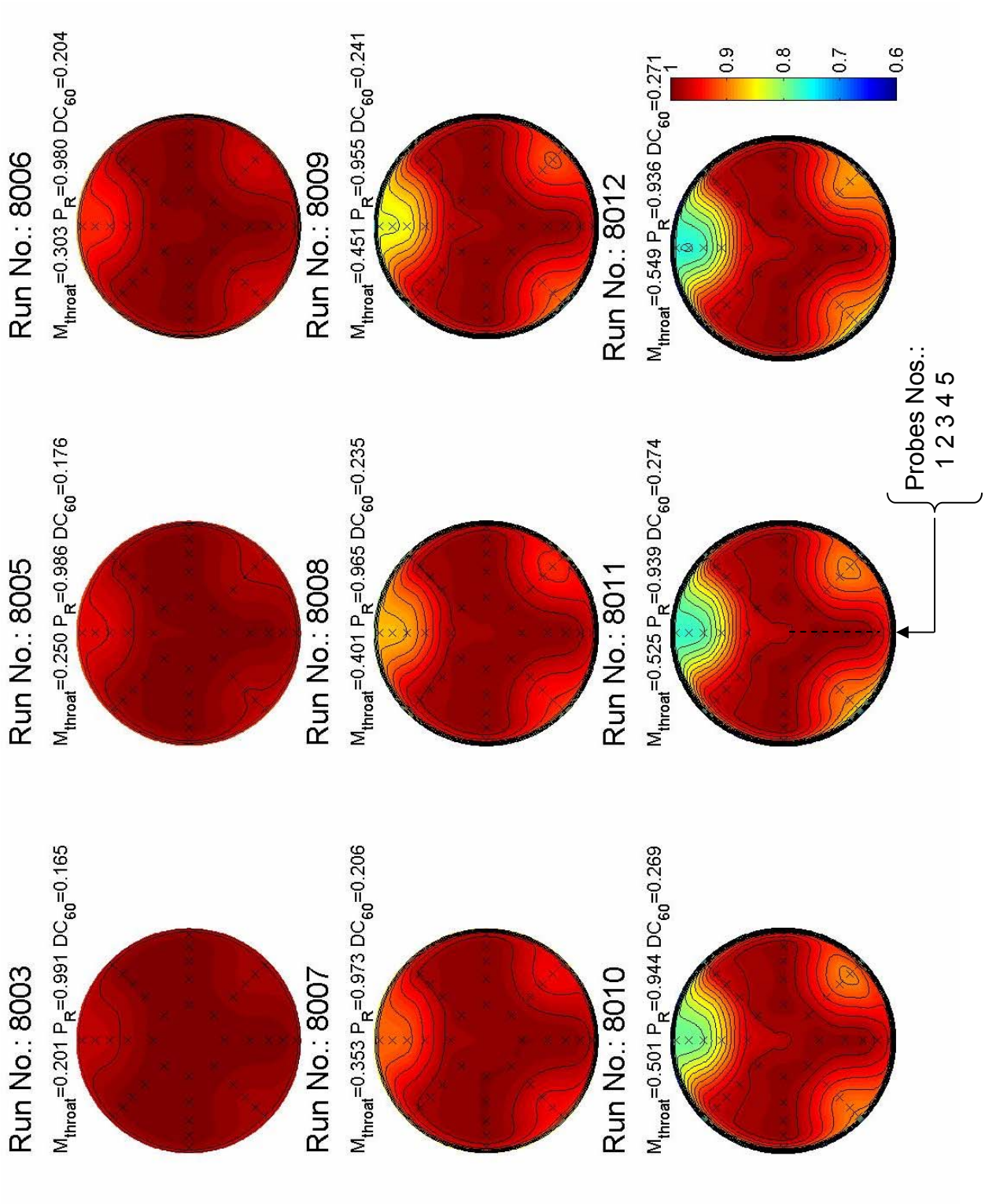

Figure 6. Total pressure distributions at the AIP at different throat Mach numbers

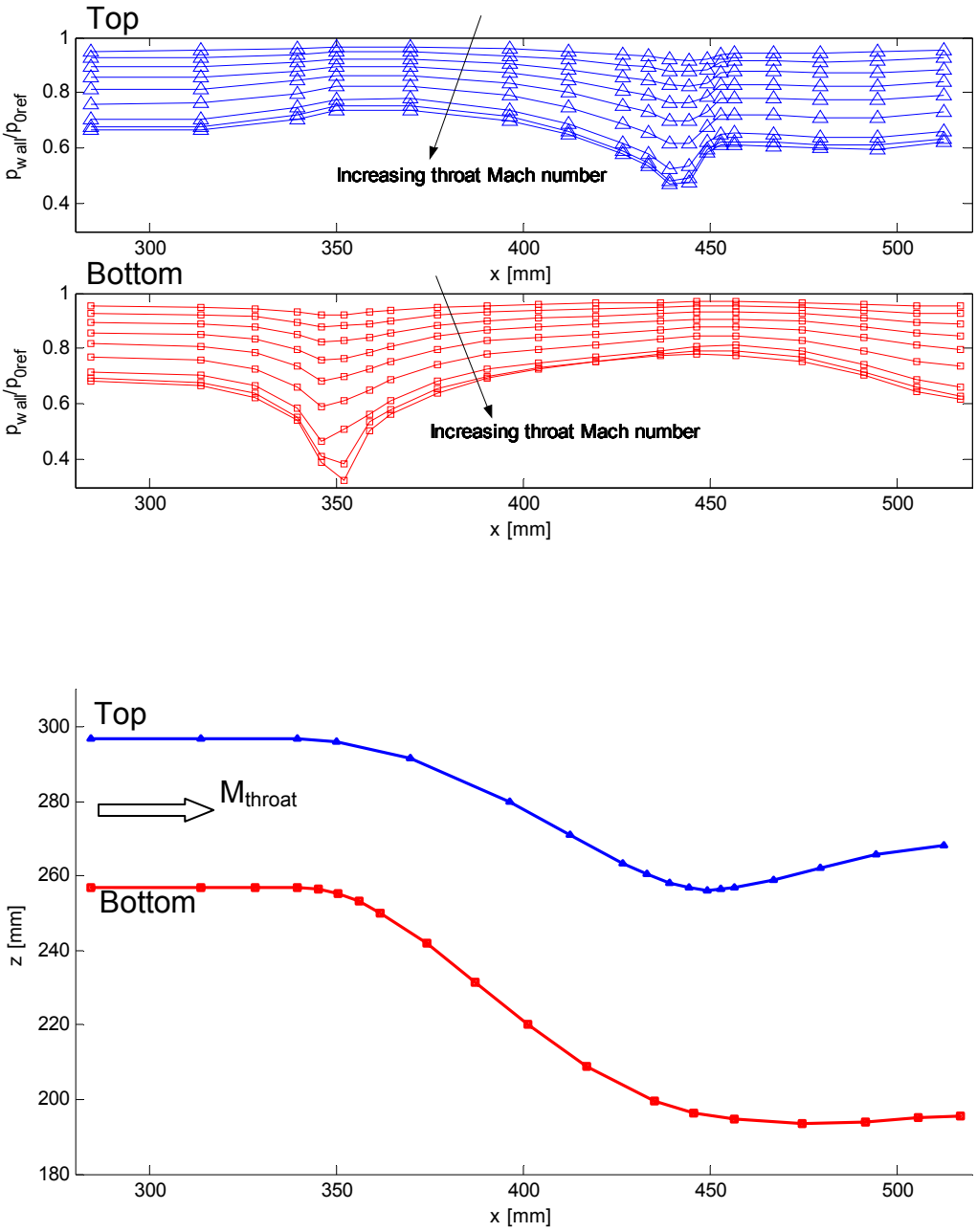

Figure 7. Static pressure distributions along top and bottom of the inlet duct at different throat Mach numbers and top and bottom static pressure tap locations

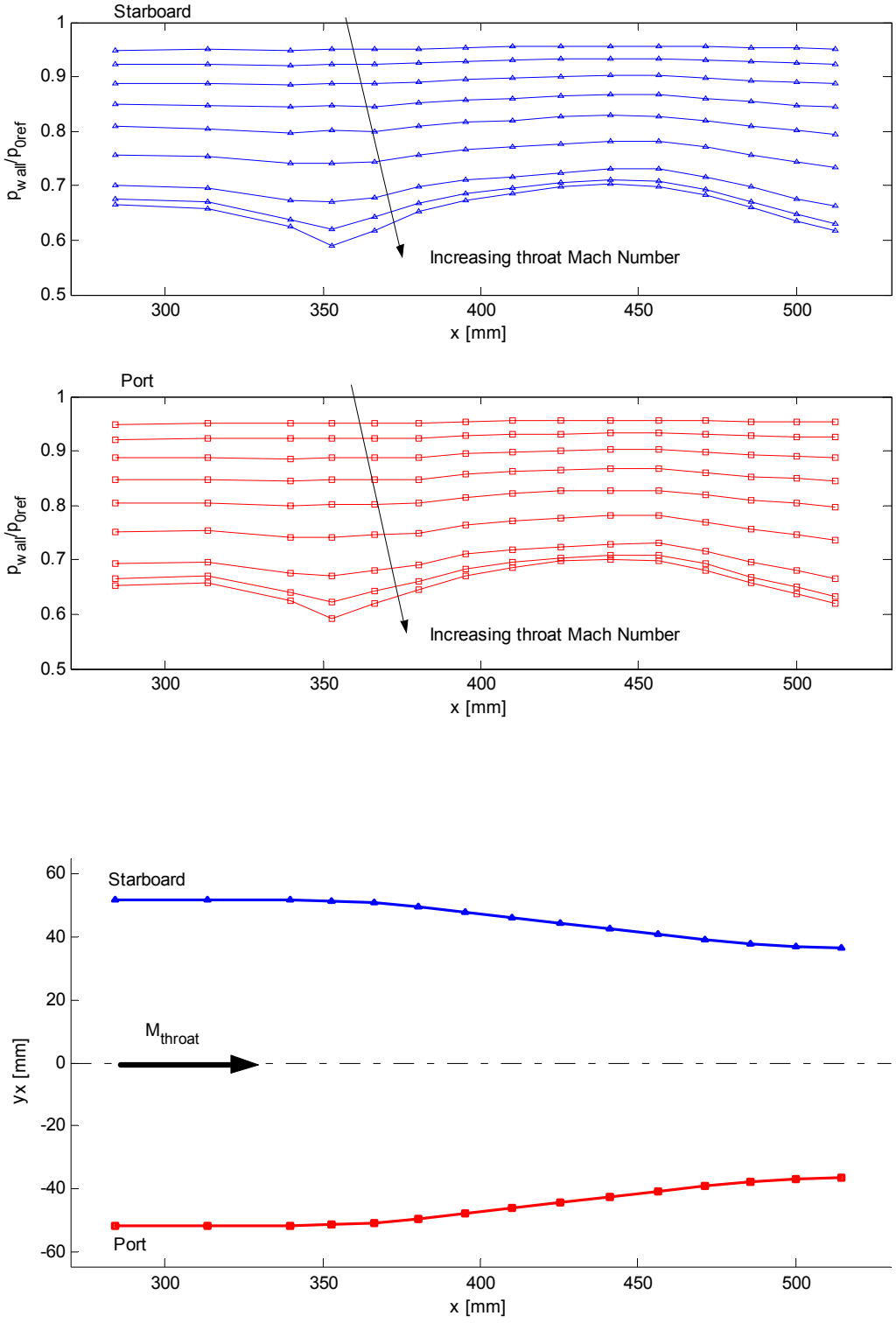

Figure 8. Static pressure distributions along the sides of the inlet duct at different throat Mach numbers and corresponding static pressure tap locations

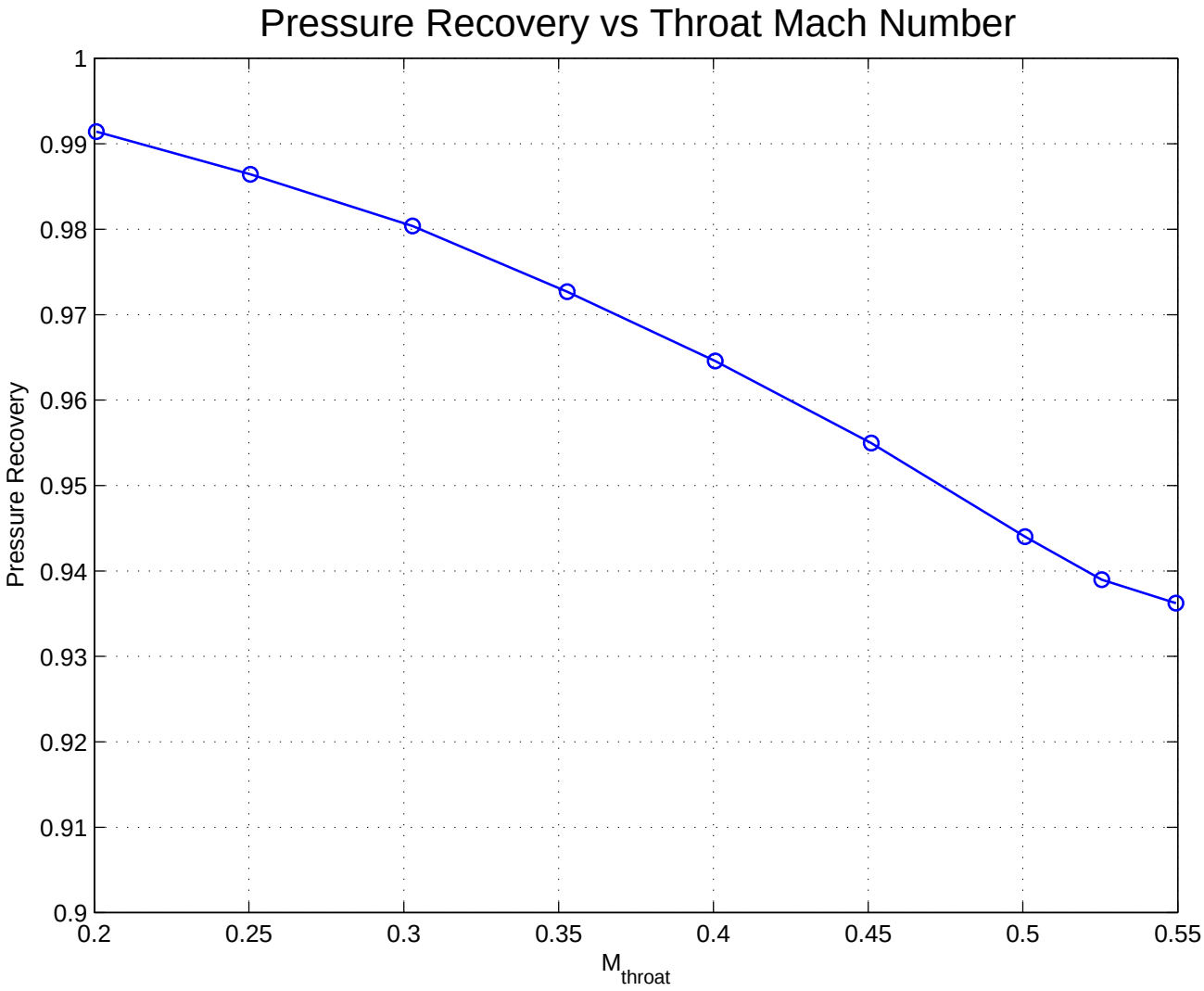

Figure 9. Pressure recovery as function of throat Mach number

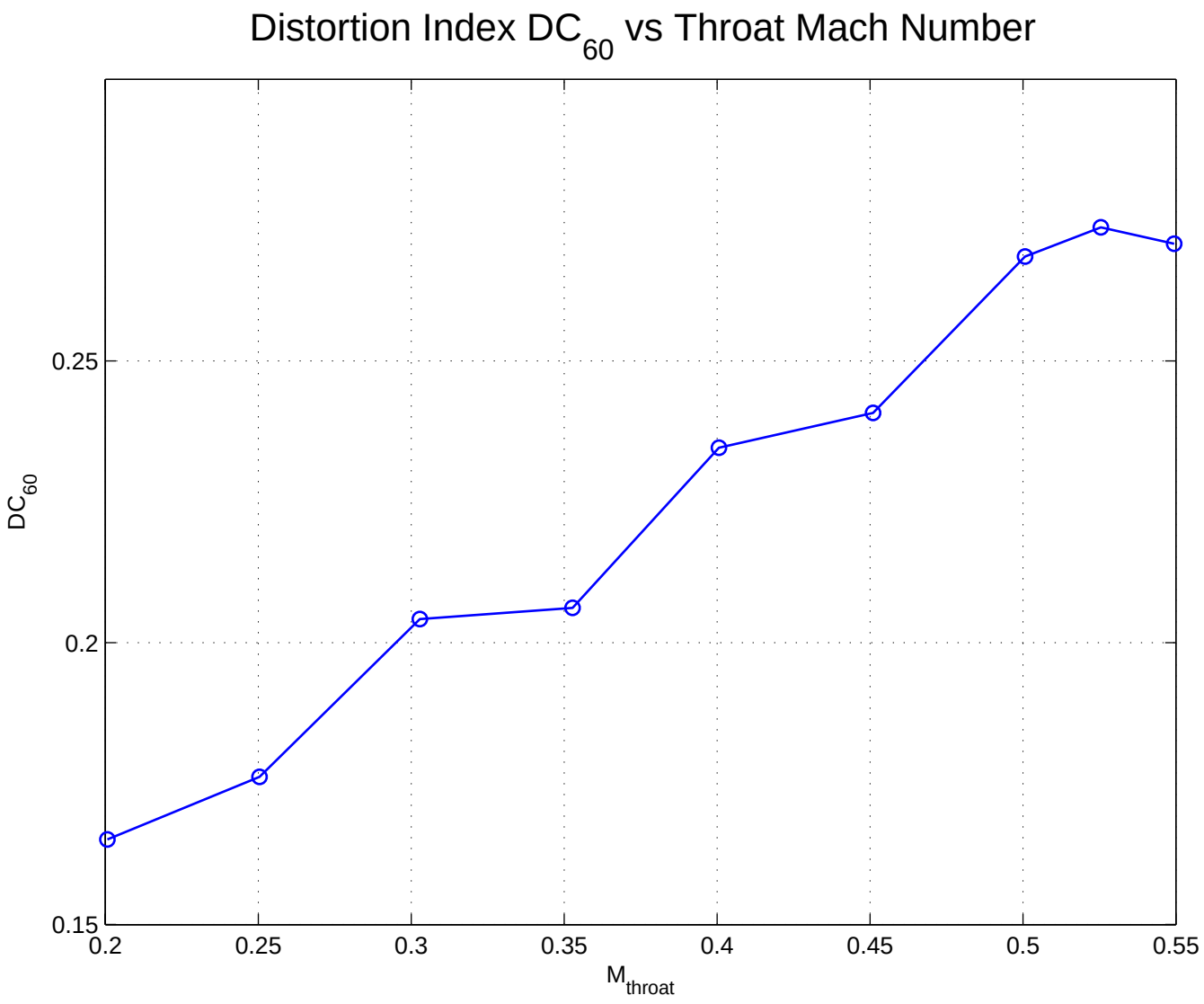

Figure 10. Distortion index DC_{60} as function of throat Mach number

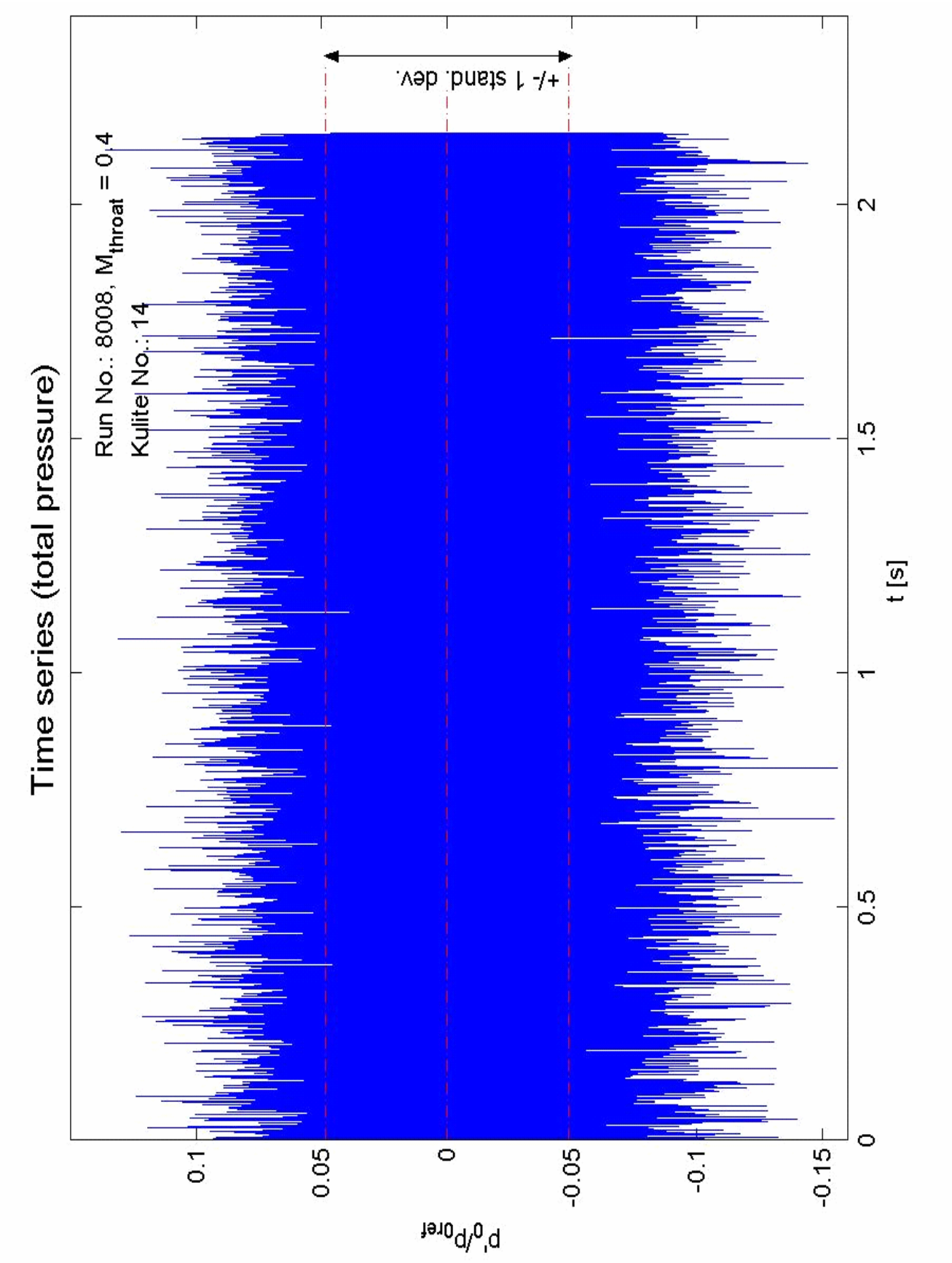

Figure 11a. Time series of total pressure (Kulite No. 14, M_{throat} = 0.4)

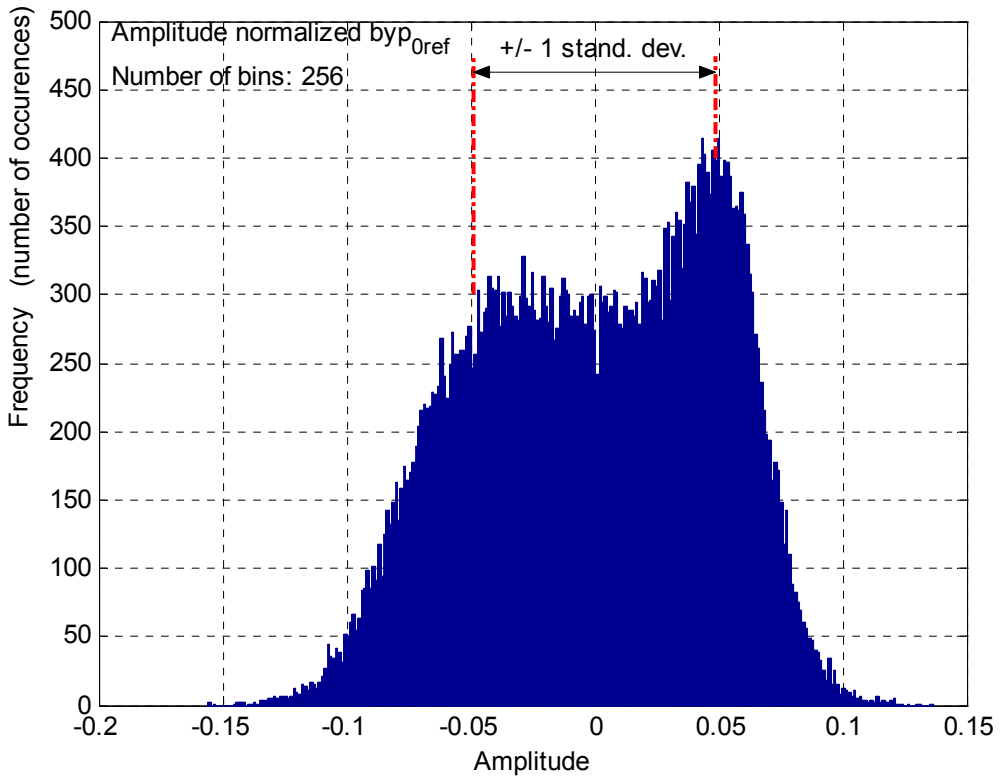

Figure 11b. Histogram of total pressure signal (Kulite No.: 14, M_{throat} = 0.4)

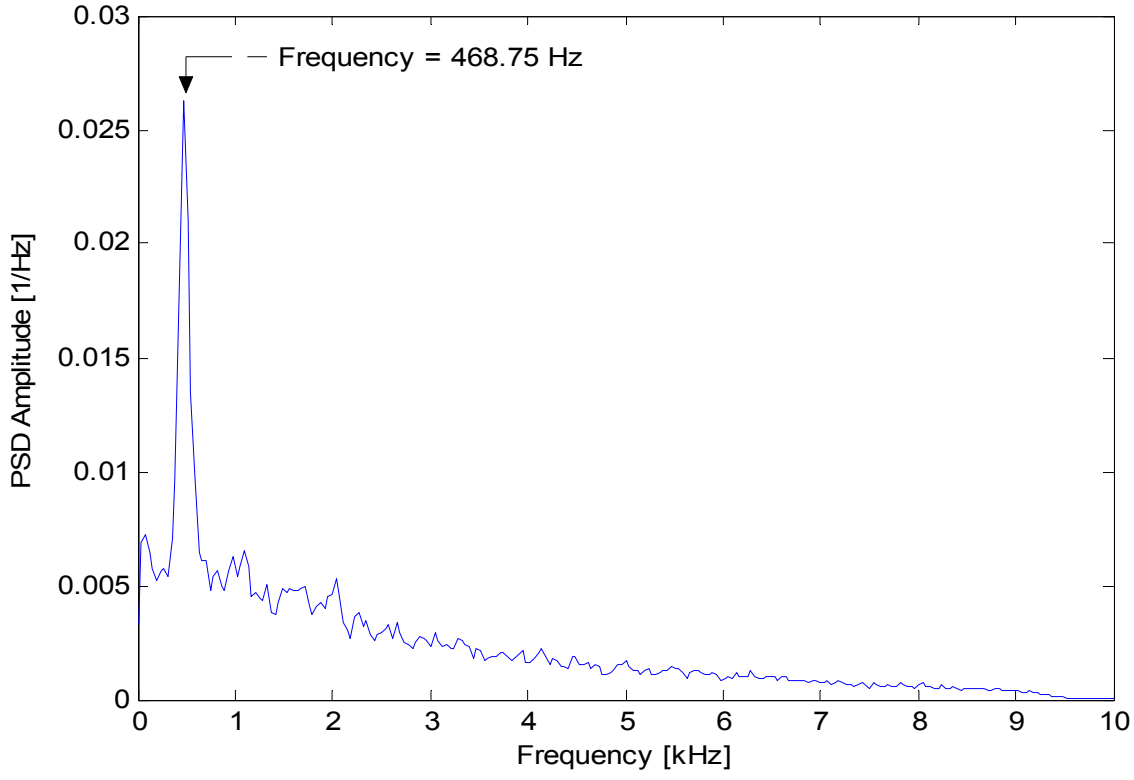

Figure 11c. Power spectral density of total pressure signal (Kulite No.: 14, M_{throat} = 0.4)

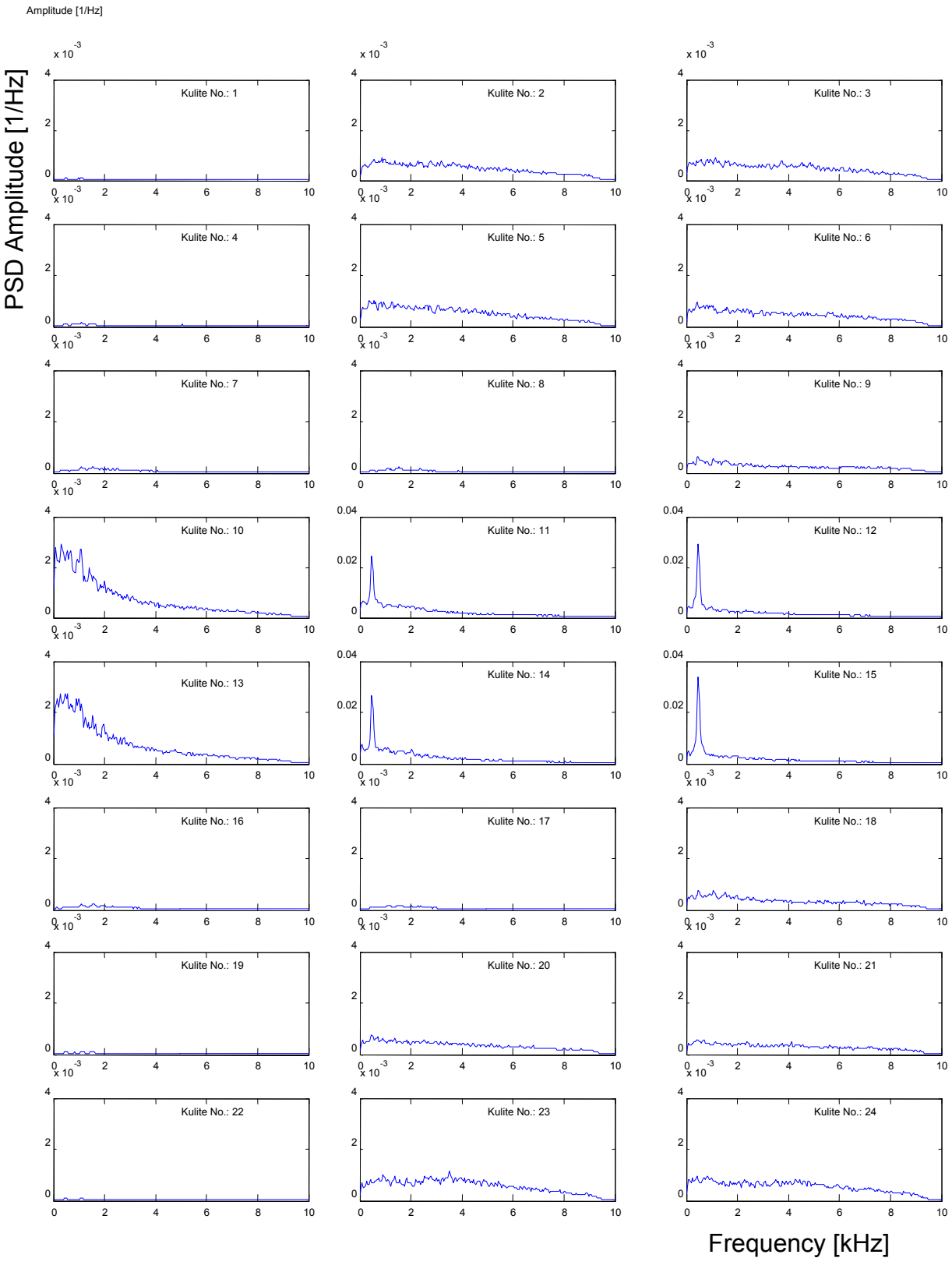

Figure 12. Subplot of all 24 Kulite total pressure PSDs (M_{throat} = 0.4)

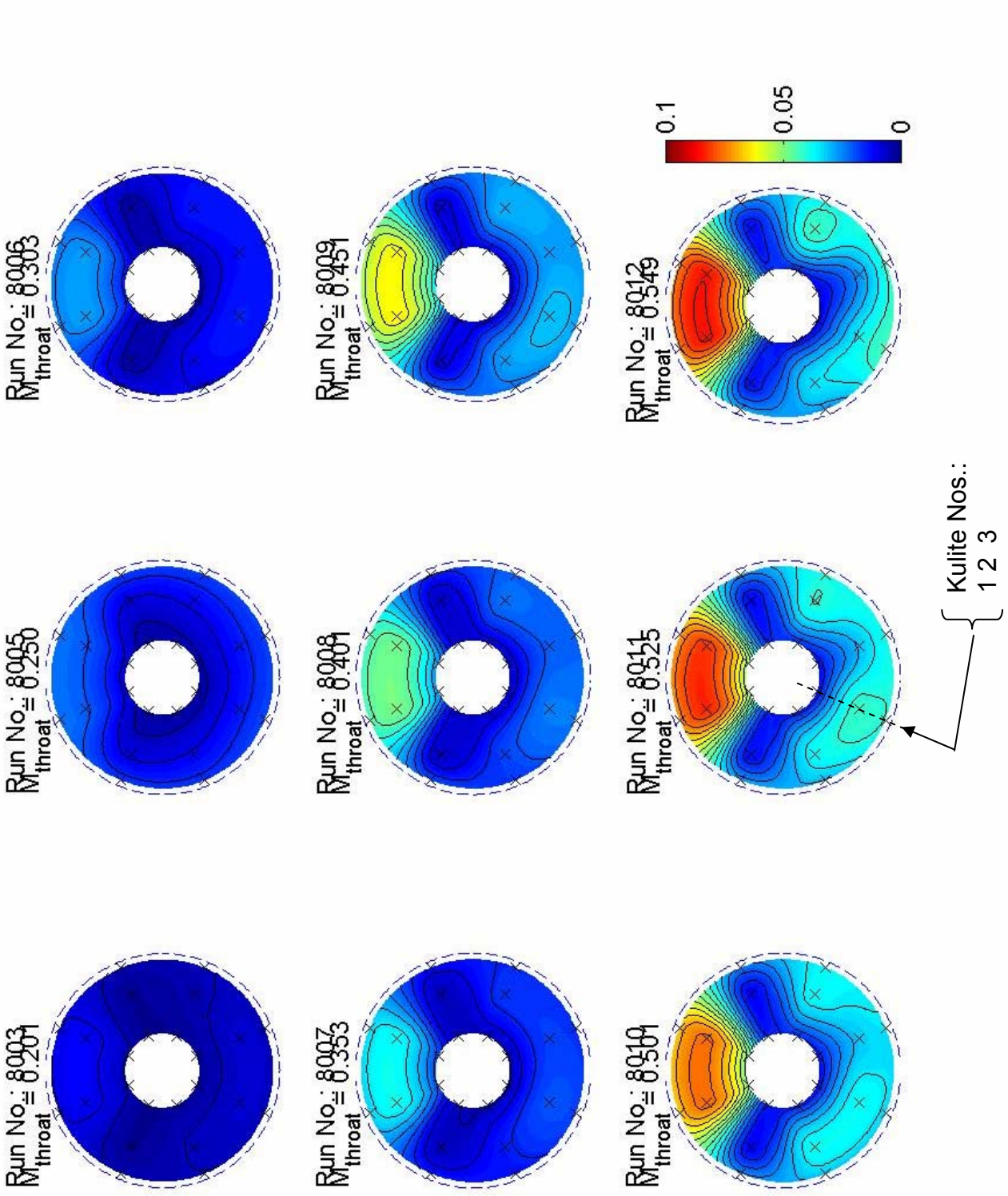

Figure 13. Distribution of time-variant total pressure RMS values at the AIP

Issuing organization
FOI – Swedish Defence Research Agency
Systems Technology
SE-164 90 Stockholm

Report number, ISRN
FOI-R--1572--SE

Report type
Technical

Research area code
7. Mobility and space technology, incl materials

Month year
November 2005

Project no.
E61101

Sub area code
72 Air vehicles

Sub area code 2

Author/s (editor/s)
Ingemar Samuelsson

Project manager
Ingemar Samuelsson

Approved by
Monica Dahlén

Sponsoring agency
FMV

Scientifically and technically responsible
David Bolander

Report title
Test of An UCAV Air Inlet Duct (Eikon) at Static Conditions in FOI Suckdown Facility

Abstract
A static test (that is, without free stream) of an UCAV air inlet duct has been carried out at the FOI S1 facility. The inlet duct model, fabricated by means a RPM technique in plastic, was in scale 1:9.05. The inlet mass flow was varied from low throat Mach number of 0.2 up to about 0.55; the flow was induced by opening the duct to an evacuated rock chamber. At the test the AIP total pressures (both steady and time-variant), inlet wall static pressures and the duct mass flow rate were measured.

It was found that the inlet pressure recovery decreased gradually from about 0.99 to about 0.94 over the tested mass flow rate range while the distortion index DC_{60} increased from about 0.17 to about 0.27 in this range. At the highest tested mass flow rates the duct flow seemed to be choked. Where this choking occurred in the duct is not known, neither is the associated fluid dynamic mechanism.

The AIP total pressure distribution indicated that the highest losses probably are associated with flow separation at the upper duct wall S-bend. In order to enhance the inlet performance it is proposed that some form of flow control is applied in this region.

Keywords
Air inlet model, static test, pressure recovery, distortion, choking, flow separation

Further bibliographic information

Language English

ISSN 1650-1942

Pages 26 p.

Price acc. to pricelist

Utgivare
FOI - Totalförsvarets forskningsinstitut
Systemteknik
164 90 Stockholm

Rapportnummer, ISRN
FOI-R--1572--SE

Klassificering
Teknisk rapport

Forskningsområde
7. Farkost- och rymdteknik, inkl material

Månad, år
November 2005

Projektnummer
E61101

Delområde
72 Luftfarkoster

Delområde 2

Författare/redaktör
Ingemar Samuelsson

Projektledare
Ingemar Samuelsson

Godkänd av
Monica Dahlén

Uppdragsgivare/kundbeteckning
FMV/FoT25

Tekniskt och/eller vetenskapligt ansvarig
David Bolander

Rapportens titel
Riggprov av ett UCAV-luftintag (Eikon) vid statiska förhållanden i FOI S1

Sammanfattning
Ett UCAV-luftintag har provats statiskt (utan friström) vid FOI:s S1-tunnel. Luftintagsmodellen, tillverkad med friformsteknik i plast, utfördes i skalan 1:9.05. Intagsmassflödet varierades från låga halsmachtal 0.2 upp till omkring 0.55.; strömningen inducerades genom att öppna kanalen mot ett evakuerat bergrum. Vid provet mättes totaltryck i AIP, både medelvärden och tidsberoende, kanalväggens statiska tryck samt massflödet genom kanalen.
Av erhållna provresultat kan t.ex. nämnas att tryckåtervinsten sjönk från ungefär 0.99 till ungefär 0.94 över det provade massflödesintervallet (från lågt till högt), medan distorsionindex DC_{60} ökade från 0.17 till omkring 0.27 i detta intervall. Vid det högsta provade massflödet tycktes kanalströmningen vara kritisk. Var denna kritiska strömning uppträdde i kanalen är inte känt, ej heller den därmed förknippade strömningsfysiken.
Fördelningen av totaltryck över AIP antyder att de största totaltrycksförlusterna troligtvis sammanhänger med strömningsavlösning vid kanalväggens övre S-krök. För att öka intagets prestanda föreslås att någon form av strömningsstyrning tillämpas i detta område.

Nyckelord
Luftintagsmodell, statiskt prov, tryckåtervinst, distorsion, kritisk strömning, strömningsavlösning

Övriga bibliografiska uppgifter

Språk Engelska

ISSN 1650-1942

Antal sidor: 26 s.

Distribution enligt missiv

Pris: Enligt prislista